Secondary eyewall formation in WRF simulations of Hurricanes Rita and Katrina (2005)

Sergio F. Abarca[1] and Kristen L. Corbosiero[1]

Received 5 February 2011; revised 1 March 2011; accepted 7 March 2011; published 7 April 2011.

[1] An analysis is presented of two high-resolution hurricane simulations of Katrina and Rita (2005) that exhibited secondary eyewall formation (SEF). The results support the notion of vortex Rossby waves (VRWs) having an important role in SEF and suggest that VRW activity is a defining aspect of the moat. SEF occurs at a radius of ~65 (80) km in Katrina (Rita), close to the hypothesized stagnation radius of VRWs. VRW activity appears to be the result of eye-eyewall mixing events, themselves a product of the release of barotropic instability. The convection in the radial region that becomes the moat is mainly in the form of VRWs propagating radially outward from the primary eyewall until the negative radial gradient of potential vorticity is no longer conducive for their propagation. These convectively coupled waves, originating and being expelled from the eyewall, are rotation dominated and have the coherency necessary to survive their passage through the strain-dominated region outside the eyewall. **Citation:** Abarca, S. F., and K. L. Corbosiero (2011), Secondary eyewall formation in WRF simulations of Hurricanes Rita and Katrina (2005), *Geophys. Res. Lett.*, *38*, L07802, doi:10.1029/2011GL047015.

1. Introduction

[2] Given their frequency of occurrence [*Kossin and Sitkowski*, 2009; *Kuo et al.*, 2009] and their relationship with storm duration [*Kuo et al.*, 2009] and intensity change [*Willoughby et al.*, 1982; *Houze et al.*, 2007], secondary eyewalls (SEs) and their formation are two of the most important research topics in the dynamics of tropical cyclones (TCs). Despite its importance, however, there is no unified theory to explain secondary eyewall formation (SEF).

[3] Highly idealized numerical frameworks have been used to propose hypotheses for SEF. Using two axisymmetric models, *Nong and Emanuel* [2003] proposed that SEF results from wind-induced surface heat exchange after being triggered by external forcing. *Kuo et al.* [2008] and *Martinez et al.* [2010] used barotropic simulations to investigate how vorticity perturbations around a strong TC-like vortex may relax to form a ring of enhanced vorticity. However, a more realistic representation of the perturbations suggests that barotropic dynamics may be an oversimplification of the SEF problem [*Moon et al.*, 2010]. Barotropic dynamics have also been used to propose concepts like the rapid filamentation zone [*Rozoff et al.*, 2006], that along with subsidence associated with the secondary circulation [*Houze et al.*, 2007], have been proposed to explain the existence of the convection free moat.

[4] High resolution, full-physics numerical simulations have also been used to study SEF. *Terwey and Montgomery* [2008] hypothesized that SEF is the product of the axisymmetrization of a jet that results from the anisotropic upscale energy cascade of convectively generated vorticity anomalies. In this view, the anisotropy is the result of a negative radial gradient of potential vorticity (PV), denoted the beta skirt. *Judt and Chen* [2010] suggested that in situ generation and accumulation of PV within the rainband region leads to a PV maximum that results in SEF. *Qiu et al.* [2010] concluded that during SEF, convection in an outer spiral rainband moved in towards the core and was axisymmetrized in the beta skirt. This region had enough radial extent to interact with the outer rainband due to previous vortex Rossby wave (VRW) activity emanating from the primary eyewall and propagating outward along the mean radial gradient of PV. Finally, *Martinez et al.* [2011] suggested a VRW-mean flow interaction mechanism for SEF based on the stagnation radius of wavenumber one VRWs (that dominated the inner core) and the radius of cessation of an outward propagating maximum of eddy angular momentum flux being located in the same radial region where SEF occurs.

[5] Here we present an analysis of two high-resolution numerical simulations that produced SEF and support the notion of VRWs having an important role in SEF. Further, the results suggest that VRW activity (and the absence of it) may be an important aspect of moat dynamics.

2. Model Setup

[6] Two integrations (carried out at the National Center for Atmospheric Research) of the Advanced Research core of the Weather Research and Forecasting (WRF) model, deemed the Advanced Hurricane WRF [*Davis et al.*, 2008], are examined. The simulations have three domains (12, 4 and 1.33 km) with two-way movable nests, Kain-Fritsch cumulus parameterization (only in the outer domain), the WRF single-moment 5-class microphysics scheme and the Yonsei University scheme for the planetary boundary layer. A model performance evaluation and further information regarding the simulations are presented by *Davis et al.* [2008].

[7] Of the two simulations presented, one, hereon denominated Katrina, was initialized at 0000 UTC 27 August 2005; the other, hereon denominated Rita, was initialized at 0000 UTC 21 September 2005. Each simulation was integrated for 72 hours. The initialization time of each simulation will be considered hour 0 and all time references

[1]Department of Atmospheric and Oceanic Sciences, University of California, Los Angeles, California, USA.

0094-8276/11/2011GL047015

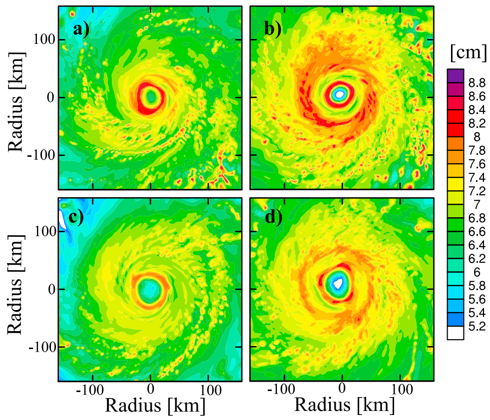

Figure 1. Precipitable water (cm) snapshots for (a) hour 20 and (b) hour 43 of Katrina, and (c) hour 20 and (d) hour 46 of Rita.

are made with respect to it. Landfall occurred in both simulations, at hour 61 (67) in Katrina (Rita).

3. Results

[8] Figure 1 (corresponding to the 1.33 km domain) shows the inner core structure of the Katrina and Rita simulations as captured by snapshots of precipitable water (PW). In the left panels, the primary eyewalls are clearly defined, centered at a radius of about 20 km in the case of Katrina (Figure 1a) and about 25 km in the case of Rita (Figure 1c). Approximately 25 hours later (Figures 1b and 1d), while still preserving its original eyewall, each storm exhibits a distinctive secondary maximum in PW centered at about the 60 km radius. In each case, a 30 to 40 km wide moat is discernible between the concentric rings of elevated PW.

[9] To show the time evolution of the simulations, hovmöller diagrams of azimuthally averaged PW, PV, vertical velocity and horizontal wind magnitude are presented in Figure 2. (The storm center was determined using the method of *Cram et al.* [2007].) Comparison of the PW (Figures 2a and 2d) and PV (Figures 2b and 2e) panels shows that the primary and secondary eyewalls are not only characterized by maxima in convective activity, but also by PV maxima in the lower troposphere. The secondary PW maxima in both storms seem to originate from emanations of high PW from the primary eyewall, e.g., at hour 30 (15) in Katrina (Rita) that stagnate at a radius of ~65 km for Katrina and about 80 km for Rita. The outward emanation of large values of PW occurs up to hour 34 in Katrina, while it stops earlier (hour 19) in Rita. After the initial period where large values of PW propagate outward from the primary eyewall, but before the SE is clearly distinguishable, the moat is clearly established as evidenced by the radially extensive regions of azimuthally averaged negative vertical velocity shown in Figures 2c and 2f.

[10] The SE is also apparent in both the increased horizontal and upward vertical components of the wind (Figures 2c and 2f). The outward expansion of the wind field seems to start several hours earlier than the development of any secondary maximum in wind magnitude. In Katrina, the secondary wind maximum develops at hour 55, while in Rita it does not occur, perhaps because the two eyewalls were too close together and merged before such configuration could be reached.

[11] While azimuthal averages of PV are useful to identify the overall structure, convective activity in the TC environment is characterized by PV dipoles (perturbations of opposite sign) that are averaged out with this statistic. Thus, enstrophy (PV variance) is a quantity better suited to identify convective activity. Figures 3b and 3d show PV enstrophy at 850 hPa and demonstrate that there is large PV variance in several regions of the storms, including the inner and outer sides of the primary eyewall, and the region where the SE is established. Large PV variance is also episodically observed in the region where PW and PV azimuthal averages show large values of these quantities propagating radially outward. In this region, the activity seems to emanate from the eyewall in discrete events corresponding to outward propagating spiral rainbands (e.g., the band ~40 km northeast of the center of Katrina in Figure 1a). The discrete events repeatedly occur up to hour 34 (19) in Katrina (Rita). After this time, the outward propagation ceases almost completely, leading to a moat-like feature outside the primary eyewall.

[12] Figures 3b and 3d also show that the inner side of the eyewall displays discrete increases in PV variance that reach into the storm center. These increases result in a temporal rearrangement of the PV configuration from a ring-like structure into a more monopolar vortex (Figures 2b and 2e), consistent with the barotropic instability and eye-eyewall mixing events described by *Schubert et al.* [1999]. To quantitatively assess the occurrence of mixing events, palinstrophy (a measure of vorticity gradients [*Rozoff et al.*, 2009]), defined as $P = \iint 1/2\ \nabla PV_{850\ hPa} \cdot \nabla PV_{850\ hPa}\ d\theta\ dr$, is integrated from the center of the storm to a subjectively determined center of convective activity in the eyewall (at a radius of 20 km for Katrina and 25 km for Rita). Figures 3a and 3c show the evolution of palinstrophy and azimuthally averaged wind speed. In both storms, maxima in palinstrophy (e.g., hour 13 (10) in Katrina (Rita)) are associated with the outward propagation of convective activity. Once the moat is established, the variability in palinstrophy continues to exhibit maxima, but the outward propagation of convective activity is mostly absent.

[13] Figure 4 shows radial profiles of azimuthally averaged PV. It shows that both simulations started with PV radial gradients that can serve as the restoring force for VRWs [*Montgomery and Kallenbach*, 1997] and that these gentle gradients were maintained until hour 34 (19) for Katrina (Rita; Figures 4a and 4d). After these times, the PV radial gradients started to exhibit a flatter structure (Figures 4b and 4e), non-conducive for VRW propagation. At later times (Figures 4c and 4f), the radial PV profiles started exhibiting the maxima associated with the SEs.

4. Discussion

[14] The results of the two simulations support the notion that SEF and the moat are intimately related to bands of high PW and PV variance emanating from the primary eyewall. The outward propagating features take the form of spiral bands and are considered to be VRWs. A complete diagnosis of VRW activity would require an analysis of the kinematics of the waves evaluated with high time resolution

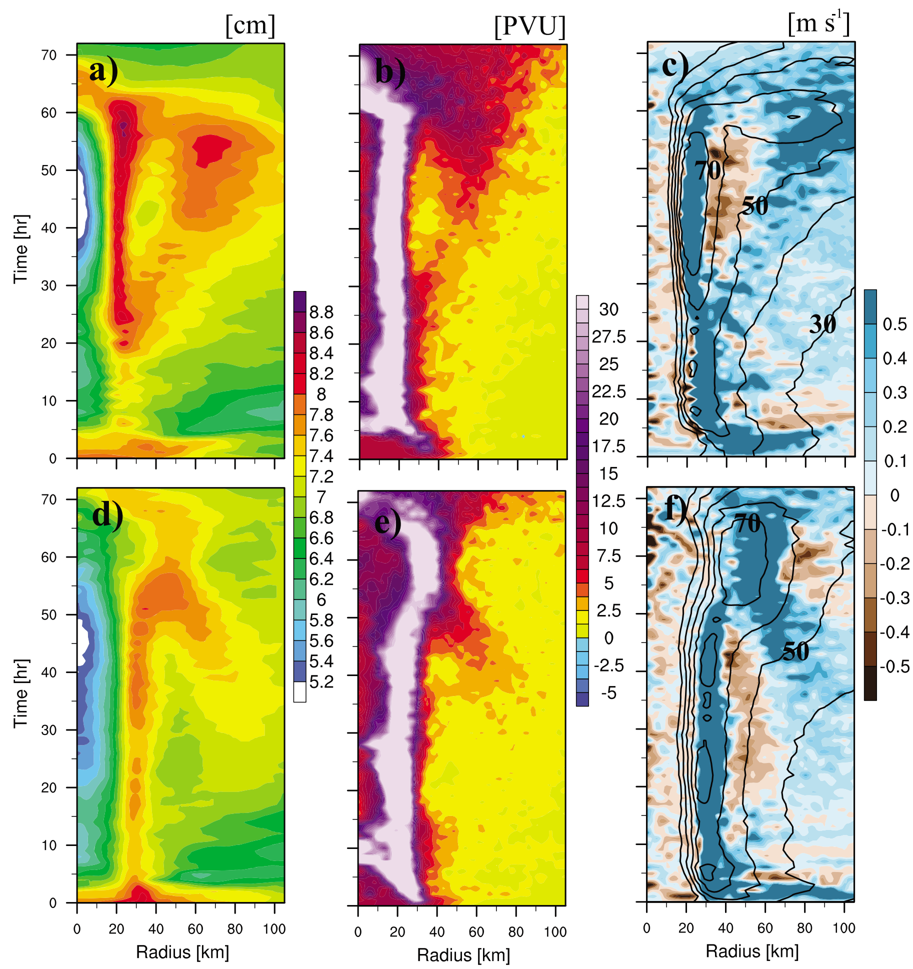

Figure 2. (a–c) Katrina and (d–f) Rita hovmöller diagrams of azimuthally averaged precipitable water (cm; Figures 2a and 2d), 850 hPa potential vorticity (PVU; Figures 2b and 2e), and 850 hPa vertical velocity (m s^{-1}, shaded) and horizontal wind magnitude (m s^{-1}, contours; Figures 2c and 2f).

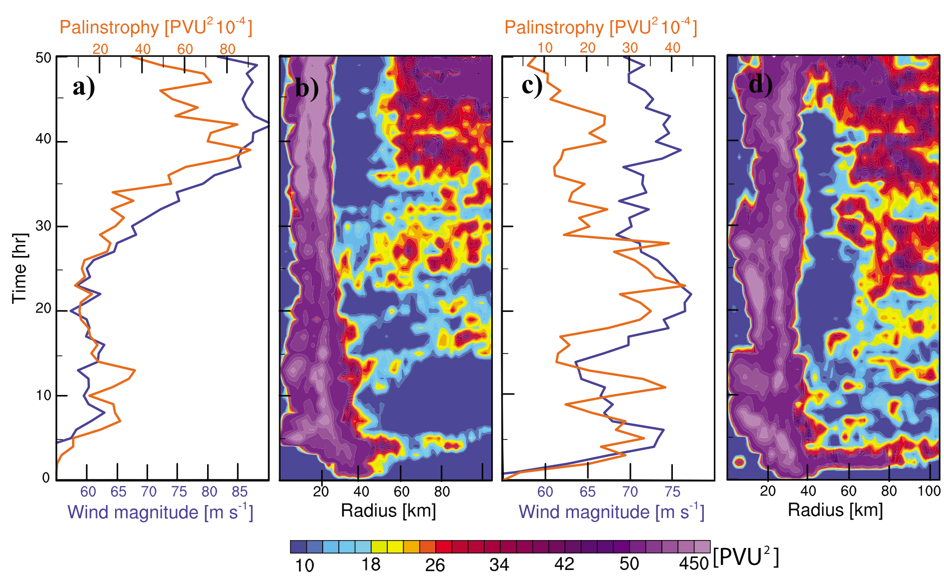

Figure 3. (a and c) Wind magnitude and palinstrophy and (b and d) PV enstrophy for Katrina (Figures 3a and 3b) and Rita (Figures 3c and 3d). All quantities are valid at 850 hPa.

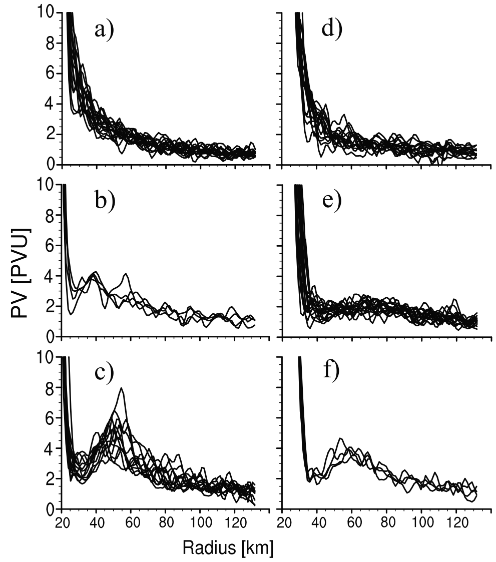

Figure 4. Azimuthally averaged radial PV profiles for (a–c) Katrina and (d–f) Rita. Hours 19 to 34 (Figure 4a) and 4 to 18 (Figure 4d); hours 35 to 38 (Figure 4b) and 19 to 34 (Figure 4e); and hours 39 to 50 (Figure 4c) and 41 to 44 (Figure 4f).

output that is not available in these simulations (the output here is hourly). However, the fact that the outward propagating features exist only when there is a gentle negative radial gradient of PV and that they have coincident maxima in PV and PW, gives confidence that the outward propagating features are indeed convectively coupled VRWs.

[15] The hypothesized VRW activity appears to be the result of eye-eyewall mixing events, themselves a product of the release of barotropic instability [*Schubert et al.*, 1999]. The discrete increases in enstrophy, seen in Figures 3b and 3d, are associated with the reconfiguration of the PV field in the inner core which transitions from a ring to more of a monopole (Figures 2b and 2e). To conserve angular momentum as this rearrangement occurs, some high eyewall PV is also mixed outward, taking the form of spiral rainbands. A comparison of Figures 3a and 3c with Figures 3b and 3d shows that inward mixing of vorticity, as captured by palinstrophy maxima at 850 hPa, is accompanied by outward propagating features (VRWs).

[16] Figures 2a, 2b, 2d, and 2e show that SEF occurs at about 65 (80) km in Katrina (Rita). This radius is close to the hypothesized stagnation radius of VRWs where the outward propagation of the waves ceases due to their increasing radial wavenumber. With the radius of maximum wind (RMW) being about 22 (27) km for Katrina (Rita), the stagnation radius in the simulations is located at a radius approximately three times the RMW, consistent with the findings of *Montgomery and Kallenbach* [1997] and *Corbosiero et al.* [2006]. Whether the role of VRWs in SEF is through wave-mean flow interaction (as described by *Martinez et al.* [2011]) and/or through the accumulation of PV at the stagnation radius is currently being investigated in higher time resolution (10 min) simulations.

[17] In addition to the link between VRWs and SEF, VRW activity also seems to be a defining aspect of the moat. The effect of filamentation in the strain dominated region outside the primary eyewall [*Rozoff et al.*, 2006] and the effects of subsidence associated with convective activity in the primary and secondary eyewalls [*Rozoff et al.*, 2008; *Houze et al.*, 2007] have been proposed to explain the lack of deep convection in the moat. Consistent with these ideas, the simulations presented here exhibit a moat free of convection characterized by filamentation times smaller than 30 min for radii less than ~50 km and downward motion (Figures 2c and 2f). However, the convection in the region that becomes the moat is mainly in the form of VRWs propagating outward from the primary eyewall. This convection, originating and propagating away from the eyewall, is rotation dominated and has the coherency necessary to survive its passage through the strain dominated flow region [*Wang*, 2008]. Thus, the occurrence of this convective activity is not necessarily only modulated by the strength of the strain deformation and subsidence, but also by the radial gradient of PV. When the radial gradient of PV is conducive for VRWs (Figures 4a and 4d), there is convection. It is only when the radial gradient of PV is not conducive for VRW propagation (Figures 4b and 4e), that convection is eliminated in the radial region of the moat.

[18] Finally, Figures 2c and 2f suggest that, at least in the cases studied, a secondary wind maximum is a late manifestation of SEF that follows a maximum in convective activity (consistent with *Judt and Chen* [2010, Figure 6]). Moreover, radius-height plots of the change in the azimuthal average wind speed with time (not shown) reveal that jet-like structures only appear after hour 50 (45) for Katrina (Rita) between the 60 and 90 km radii and below 2 km. This acceleration begins after the wind field of each storm has already expanded radially (Figures 2c and 2f) and after the moat has started to be defined; i.e., a jet-like acceleration associated with SEF starts at a time when the PV radial gradients were flat and not conducive for VRW propagation. These profiles are also not conducive for the anisotropic energy cascade that could develop a finite-amplitude lower tropospheric jet as *Terwey and Montgomery* [2008] suggested, casting doubt on the SEF mechanism they proposed.

[19] **Acknowledgments.** The authors wish to thank the Hurricane Group in the Mesoscale and Microscale Meteorology Division at the National Center for Atmospheric Research (of which the second author was a member while an Advanced Study Program Postdoctoral Fellow from 2005 to 2007). Specifically, we thank Wei Wang, Chris Davis, and Greg Holland for their model guidance and discussions. We would like to acknowledge high performance computing support provided by NCAR's Computational and Information Systems Laboratory, sponsored by the National Science Foundation. We also thank two anonymous reviewers for their careful reading of the manuscript and helpful suggestions.

[20] The Editor thanks the two anonymous reviewers.

References

Corbosiero, K. L., J. Molinari, A. R. Aiyyer, and M. L. Black (2006), The structure and evolution of Hurricane Elena (1985). Part II: Convective asymmetries and evidence for vortex Rossby waves, *Mon. Weather Rev.*, *134*, 3073–3091, doi:10.1175/MWR3250.1.

Cram, T. A., J. Persing, M. T. Montgomery, and S. A. Braun (2007), A Lagrangian trajectory view on transport and mixing processes between the eye, eyewall, and environment using a high- resolution simulation of Hurricane Bonnie (1998), *J. Atmos. Sci.*, *64*, 1835–1856, doi:10.1175/JAS3921.1.

Davis, C., et al. (2008), Prediction of landfalling hurricanes with the advanced hurricane WRF model, *Mon. Weather Rev.*, *136*, 1990–2005, doi:10.1175/2007MWR2085.1.

Houze, R. A., Jr., S. S. Chen, B. F. Smull, W.-C. Lee, and M. M. Bell (2007), Hurricane intensity and eyewall replacement, *Science*, *315*, 1235–1239, doi:10.1126/science.1135650.

Judt, F., and S. S. Chen (2010), Convectively generated potential vorticity in rainbands and formation of the secondary eyewall in Hurricane Rita of 2005, *J. Atmos. Sci.*, *67*, 3581–3599, doi:10.1175/2010JAS3471.1.

Kossin, J. P., and M. Sitkowski (2009), An objective model for identifying secondary eyewall formation in hurricanes, *Mon. Weather Rev.*, *137*, 876–892, doi:10.1175/2008MWR2701.1.

Kuo, H.-C., W. H. Schubert, C.-L. Tsai, and Y.-F. Kuo (2008), Vortex interactions and barotropic aspects of concentric eyewall formation, *Mon. Weather Rev.*, *136*, 5183–5198, doi:10.1175/2008MWR2378.1.

Kuo, H.-C., C.-P. Chang, Y.-T. Yang, and H.-J. Jiang (2009), Western North Pacific typhoons with concentric eyewalls, *Mon. Weather Rev.*, *137*, 3758–3770, doi:10.1175/2009MWR2850.1.

Martinez, Y., G. Brunet, and M. K. Yau (2010), On the dynamics of two-dimensional hurricane-like concentric rings vortex formation, *J. Atmos. Sci.*, *67*, 3253–3268, doi:10.1175/2010JAS3500.1.

Martinez, Y., G. Brunet, M. K. Yau, and X. Wang (2011), On the dynamics of concentric eyewall genesis: Space-time empirical normal modes diagnosis, *J. Atmos. Sci.*, in press.

Montgomery, M. T., and R. J. Kallenbach (1997), A theory for vortex Rossby waves and its application to spiral bands and intensity changes in hurricanes, *Q. J. R. Meteorol. Soc.*, *123*, 435–465, doi:10.1002/qj.49712353810.

Moon, Y., D. S. Nolan, and M. Iskandarani (2010), On the use of two-dimensional incompressible flow to study secondary eyewall formation in tropical cyclones, *J. Atmos. Sci.*, *67*, 3765–3773, doi:10.1175/2010JAS3615.1.

Nong, S., and K. Emanuel (2003), A numerical study of the genesis of concentric eyewalls in hurricanes, *Q. J. R. Meteorol. Soc.*, *129*, 3323–3338, doi:10.1256/qj.01.132.

Qiu, X., Z.-M. Tan, and Q. Xiao (2010), The roles of vortex Rossby waves in hurricane secondary eyewall formation, *Mon. Weather Rev.*, *138*, 2092–2109, doi:10.1175/2010MWR3161.1.

Rozoff, C. M., W. H. Schubert, B. McNoldy, and J. P. Kossin (2006), Rapid filamentation zones in intense tropical cyclones, *J. Atmos. Sci.*, *63*, 325–340, doi:10.1175/JAS3595.1.

Rozoff, C. M., W. H. Schubert, and J. P. Kossin (2008), Some dynamical aspects of hurricane eyewall replacement cycles, *Q. J. R. Meteorol. Soc.*, *134*, 583–593, doi:10.1002/qj.237.

Rozoff, C. M., J. P. Kossin, W. H. Schubert, and P. Mulero (2009), Internal control of hurricane intensity variability: The dual nature of potential vorticity mixing, *J. Atmos. Sci.*, *66*, 133–147, doi:10.1175/2008JAS2717.1.

Schubert, W. H., M. T. Montgomery, R. K. Taft, T. A. Guinn, S. R. Fulton, J. P. Kossin, and J. P. Edwards (1999), Polygonal eyewalls, asymmetric eye contraction, and potential vorticity mixing in hurricanes, *J. Atmos. Sci.*, *56*, 1197–1223, doi:10.1175/1520-0469(1999)056<1197:PEAECA>2.0.CO;2.

Terwey, W. D., and M. T. Montgomery (2008), Secondary eyewall formation in two idealized, full-physics modeled hurricanes, *J. Geophys. Res.*, *113*, D12112, doi:10.1029/2007JD008897.

Wang, Y. (2008), Rapid filamentation zone in a numerically simulated tropical cyclone, *J. Atmos. Sci.*, *65*, 1158–1181, doi:10.1175/2007JAS2426.1.

Willoughby, H. E., J. A. Clos, and M. G. Shoreibah (1982), Concentric eye walls, secondary wind maxima, and the evolution of the hurricane vortex, *J. Atmos. Sci.*, *39*, 395–411, doi:10.1175/1520-0469(1982)039<0395:CEWSWM>2.0.CO;2.

S. F. Abarca and K. L. Corbosiero, Department of Atmospheric and Oceanic Sciences, University of California, 405 Hilgard Ave., Los Angeles, CA 90095, USA. (abarcas@atmos.ucla.edu)